Monte Carlo simulations of the charged boson fluid at $T=0$

S. Moroni, S. Conti, and M. P. Tosi
Istituto Nazionale di Fisica della Materia and Classe di Scienze, Scuola Normale Superiore, Piazza dei Cavalieri 7, I-56126 Pisa, Italy
(Received 5 September 1995)

The diffusion Monte Carlo (DMC) method is used to analyze various properties of the three-dimensional plasma of charged bosons in the homogeneous fluid regime, over the density range $1 \leqslant r_s \leqslant 160$ extending from the so-called uniform limit ($r_s < 1$) to the crystalline phase ($r_s > 160$). The data on the static density response function $\chi(k)$ extend to intermediate and high wave number k the work of Sugiyama, Bowen, and Alder [Phys. Rev. B **46**, 13 042 (1992)] and allow us to extract the static local-field factor $G(k)$ for exchange and correlation. The DMC results for the momentum distribution $n(k)$ show that the condensate fraction decreases with increasing coupling strength from 83% at $r_s = 1$ to less than 1% at $r_s = 160$. We also present results for the ground-state energy $E_g(r_s)$ and for the structure factor $S(k)$. The results for $E_g(r_s)$, $n(k)$, and $\chi(k)$ are summarized in analytic interpolation formulas embodying the known asymptotic behaviors. A rigorous upper bound on the plasmon dispersion curve is obtained from the DMC data through a sum-rule argument.

I. INTRODUCTION

The fluid of pointlike spinless charged bosons embedded in a uniform neutralizing background has drawn some attention in the literature as a model in quantum statistical mechanics having a close relationship with the physically more relevant fermionic gas of electrons.[1–3] Its role as a primitive model for the theory of superconductivity was pointed out in the early days by Schafroth[4] and has recently attracted renewed interest in connection with ceramic superconducting materials.[5] The charged boson fluid may also have astrophysical relevance in relation to cores of white dwarf stars consisting of pressure-ionized helium.[6]

On the theoretical side, early evaluations of the ground-state energy and the spectrum of elementary excitations in the high-density limit[7–9] were followed by variational calculations of the ground state over a wide range of r_s using Jastrow wave functions.[2,3,10,11] The hypernetted-chain approximation in the Jastrow theory has been used by Saarela[12] to evaluate the static linear density response function at $T=0$. Hore and Frankel[13] had earlier given a full analytic evaluation of the dynamic dielectric function $\epsilon(k,\omega)$ of the fluid at arbitrary temperature within the random phase approximation (RPA). This approximation appears to be particularly restrictive for the fluid of interacting bosons at zero temperature, where the ideal boson gas is fully condensed in the zero-momentum state. The role of correlations beyond the RPA has been explored by Caparica and Hipolito[14] and by Gold[15] within the so-called STLS (Singwi-Tosi-Land-Sjölander) approximation as proposed earlier for the electron fluid. A more extensive study of exchange and correlation has been given by Conti, Chiofalo, and Tosi.[16]

Quantum Monte Carlo studies of the boson ground-state energy[3,17] have revealed three distinct physical regimes, depending on the dimensionless length parameter $r_s = r_0/a_0$, where r_0 is related to the particle number density ρ by $r_0 = (4\pi\rho/3)^{-1/3}$ and a_0 is the Bohr radius. The fluid at $r_s \ll 1$ is a weakly coupled gas. The role of correlations increases with decreasing density, leading to a strongly coupled liquid which eventually undergoes Wigner crystallization at $r_s \simeq 160$. This scenario parallels the behavior shown by the fluid of charged fermions.

More recently, the static dielectric function $\epsilon(k,0)$ has been directly determined by Monte Carlo methods.[18] Data on the pair distribution function $g(r)$ are also available.[19]

The main purpose of this work is to present extensive results on the static dielectric function, which has been studied earlier in a very limited range of wave numbers, and on the momentum distribution, for which the only published results have come from variational Monte Carlo.[3] In addition, we present structural and thermodynamic data over a wide range of densities.

II. METHOD

Diffusion Monte Carlo (DMC) is a well established technique for studying static ground-state properties of quantum many-body systems. Its appeal lies in that it yields *exact* predictions for a number of quantities, subject only to known statistical errors. In particular, bosonic ground-state energies and derived quantities are exact. Other properties, such as the structure factor and the momentum distribution, though biased by a trial wave function introduced for computational convenience, are nevertheless extremely accurate provided the trial function is a good approximation to the true ground state. We refer to the literature[20,21] for the details of the method. Here we only summarize a few essential notions with the aim of characterizing the accuracy of the results to be presented in the later sections.

The DMC procedure basically simulates the Schrödinger equation in imaginary time for a system of N particles as a diffusion equation, yielding a set of configurations $\{R_i\}$ sampled from the mixed distribution $p(R) = \Phi_0(R)\Psi(R) / \int dR \Phi_0(R)\Psi(R)$. Here Φ_0 is the exact bosonic ground state and Ψ is an explicitly known positive trial function, introduced to improve computational efficiency through importance sampling. By R we denote the coordinates $\mathbf{r}_1, \ldots, \mathbf{r}_N$ of all the particles. The configurations sampled from the mixed distribution $p(R)$ allow the evaluation of mixed expectation values of quantum operators,

$$A_{\rm mix}=\frac{\langle\Phi_0|A|\Psi\rangle}{\langle\Phi_0|\Psi\rangle}\simeq\frac{1}{M}\sum_{i=1}^{M}A_L(R_i), \tag{2.1}$$

where $A_L(R)=A\Psi(R)/\Psi(R)$.

The most important example is when A is the Hamiltonian. The quantity to be averaged, called the local energy, reads explicitly

$$A_L(R)=\frac{H\Psi(R)}{\Psi(R)}=-\frac{\hbar^2}{2m}\left[\sum_{i=1}^{N}\nabla_i^2\ln\Psi(R)+\left(\sum_{i=1}^{N}\nabla_i\ln\Psi(R)\right)^2\right]+\sum_{i<j}v_c(|\mathbf{r}_i-\mathbf{r}_j|), \tag{2.2}$$

$v_c(r)$ being the Coulomb potential. By averaging the local energy one obtains an estimate of the ground-state energy, which is subject only to a known statistical error.

The statistical uncertainty comes about because of the finite number M of configurations in the sampling. It can be made arbitrarily small for sufficiently long runs provided $A_L(R)$ has a finite variance. Our runs typically consist of 200 000 Monte Carlo moves after equilibration, a move being an attempt to displace simultaneously all the particles followed by a Metropolis test.[20] The trial function is of the pair product (Jastrow) form $\Psi(R)=\exp[-\Sigma_{i<j}u(|\mathbf{r}_i-\mathbf{r}_j|)]$, with $u(r)$ the RPA pseudopotential chosen according to Ref. 22.

The imaginary time evolution in the simulation, i.e., the Monte Carlo move, is generated by a short time approximation of the many-body Green function: this causes a finite time step error, which in principle can be extrapolated out by doing simulations with various time steps. In practice we have used a very small time step (ranging from 0.015 Ry^{-1} for $r_s=1$ to 45 Ry^{-1} for $r_s=160$) and verified that the time step effect is not larger than the statistical error for the quantities we measure.

Of course, simulations can only include a finite number of particles. The infinite system is represented by N particles in a cubic box of side $L=(N/\rho)^{1/3}$ with periodic boundary conditions, and the Coulomb interactions are treated by the Ewald technique, which splits the potential in a short-range part to be computed exactly in real space and a long-range part to be represented by k-space sums.[22,23] The accuracy of the procedure depends on the k-space cutoff and on the particular choice for the splitting of the original potential. We have performed simulations with 200 particles, using 20 stars of the reciprocal lattice vectors of the simulation box and the calculated Madelung constant is accurate to 1 part in 2×10^5. Ewald sums have been used to compute the pseudopotential $u(r)$ as well. We have corrected for the remaining size effect on the energy by assuming $E(\infty)=E(N)+A(r_s)/N$, where $A(r_s)$ is determined by fitting variational Monte Carlo (VMC) energies[22] obtained with different numbers of particles, ranging from 27 to 300 (this procedure assumes that the size effect is the same in VMC and DMC).

In the case of operators not having Φ_0 as an eigenstate (all but the Hamiltonian in the present context), we have calculated the *extrapolated estimator* $A_{\rm ext}=2A_{\rm mix}-A_{\rm var}$, where $A_{\rm var}=\langle\Psi|A|\Psi\rangle/\langle\Psi|\Psi\rangle$ is obtained by an independent VMC simulation.[24] The difference between the extrapolated estimator and the true ground-state expectation value $\langle\Phi_0|A|\Phi_0\rangle/\langle\Phi_0|\Phi_0\rangle$ is of second order in δ, with $\Psi=\Phi_0+\delta\Phi$, whereas the bias in the mixed estimator itself is of first order in δ.

Quantities which can be routinely computed by this scheme include (i) kinetic and potential energies obtained from the corresponding terms in the local energy, (ii) the pair distribution function,

$$g(r)=\frac{1}{N\rho}\sum_{i\neq j}\langle\delta(|\mathbf{r}_i-\mathbf{r}_j-\mathbf{r}|)\rangle, \tag{2.3}$$

and (iii) the one-body density matrix

$$n(r)=\left\langle\frac{\Psi(\mathbf{r}_1,\ldots,\mathbf{r}_i+\mathbf{r},\ldots,\mathbf{r}_N)}{\Psi(\mathbf{r}_1,\ldots,\mathbf{r}_i,\ldots,\mathbf{r}_N)}\right\rangle. \tag{2.4}$$

In these equations $\langle\ldots\rangle$ denotes the average over the configurations $\{R_i\}$ sampled either from $\Phi_0\Psi$ or from Ψ^2 (in DMC and VMC, respectively). The displacement $\mathbf{r}$ in Eq. (2.4) can be chosen either by taking fixed increments along a prescribed direction or randomly in the simulation box. The two methods give more accurate results at small and large r, respectively. In particular the former gives a precise value for the curvature of $n(r)$ at $r=0$. This provides a useful check of internal consistency for the simulation, as the kinetic energy, which is also calculated directly, is proportional to $d^2n(r)/dr^2|_{r=0}$. By Fourier transform of the one-body density matrix one obtains the momentum distribution $n(k)$. This quantity can also be computed directly at reciprocal lattice vectors of the simulation box by

$$n(k)=\left\langle\exp(-i\mathbf{k}\cdot\mathbf{r})\frac{\Psi(\mathbf{r}_1,\ldots,\mathbf{r}_i+\mathbf{r},\ldots,\mathbf{r}_N)}{\Psi(\mathbf{r}_1,\ldots,\mathbf{r}_i,\ldots,\mathbf{r}_N)}\right\rangle. \tag{2.5}$$

Here $\mathbf{r}$ is a random displacement, and the average $\langle\ldots\rangle$ extends to $\mathbf{r}$. We also average over $\mathbf{k}$ vectors of equal length.

Among the quantities to be discussed in the following sections, the extrapolated estimator $\langle ke\rangle$ of the kinetic energy has the largest error compared to statistical noise. For instance, using the pair product trial function we get $\langle ke\rangle=0.000\,472(1)$ at $r_s=160$, which is as much as 10% off the exact value of 0.000 517 as derived from the total energy via the virial theorem (see Sec. III A). The bias on the extrapolated estimators can be reduced using better trial functions: for the case of 64 particles at $r_s=160$, we have optimized numerically a trial function with both pair and triplet correlations. This improvement brings into agreement the extrapolated estimator of the kinetic energy with the exact value. However, in this paper we are concerned mainly with the dielectric response and the momentum distribution. The former is not affected by the choice of the trial function because it is computed from total energies as we explain shortly, and the latter does not change appreciably in going to the better wave function in the case mentioned above. For this reason we have used the simple pair trial function with an RPA pseudopotential in all our simulations.

The calculation of the static dielectric response $\epsilon(k,0)$ follows a somewhat different procedure.[25,18] We obtain

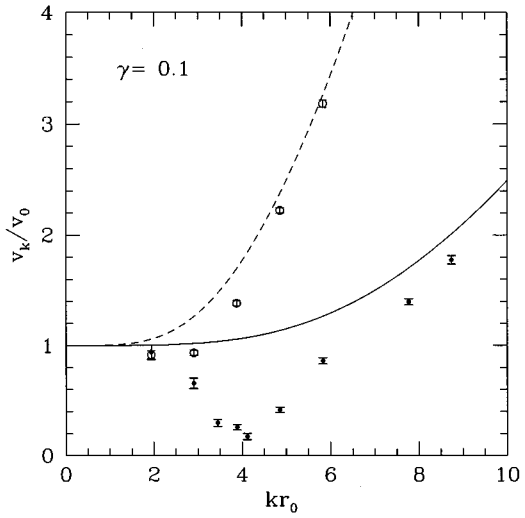

FIG. 1. External field strength $v_{\mathbf{k}}$ for which the optimal value of the variational parameter in the one-body factor is $\gamma=0.1$, for $r_s=10$ (dashed line and circles) and $r_s=160$ (full line and dots). The curves represent the RPA prediction, while the points are the result of variational minimization.

$\epsilon(k,0)$ from the static linear density response function $\chi(k)$ via the relationship $1/\epsilon(k,0)=1+v_c(k)\chi(k)$, where $v_c(k)=4\pi e^2/k^2$ is the Coulomb coupling. In evaluating $\chi(k)$ one perturbs the otherwise homogeneous many-body system with a static external potential

$$v_{\text{ext}}(\mathbf{r})=2v_{\mathbf{k}}\cos(\mathbf{k}\cdot\mathbf{r}). \tag{2.6}$$

This induces a modulation of the density with respect to its mean value ρ and a shift of the ground-state energy per particle, which can be written as

$$E_v=E_0+\frac{\chi(k)}{\rho}v_{\mathbf{k}}^2+\frac{\chi^{(3)}(\mathbf{k},\mathbf{k},-\mathbf{k})}{4\rho}v_{\mathbf{k}}^4+\cdots, \tag{2.7}$$

with $\chi^{(3)}$ the cubic response function. DMC allows one to evaluate E_v for given $\mathbf{k}$ and $v_{\mathbf{k}}$ and by performing simulations at a few coupling strengths $v_{\mathbf{k}}$ one can extract $\chi(k)$ as well as higher-order response functions from the calculated E_v by fitting in powers of $v_{\mathbf{k}}$.

At variance with other simulations performed in this work, for the very time-consuming calculation of $\epsilon(k,0)$ we have used only 64 particles. Size effects on the energy difference between the homogeneous and the modulated system have been shown to be very small in Ref. 18.

For the modulated systems the trial function is multiplied by a one-body factor $\Pi_i\exp[-\gamma\cos(\mathbf{k}\cdot\mathbf{r}_i)]$, where the amplitude γ of the density modulation is determined by variational minimization. We show in Fig. 1 the external field strength $v_{\mathbf{k}}$ for which $\gamma=0.1$ is the optimal parameter. For large r_s and $kr_0\sim4$ the RPA prediction used in Ref. 18 is far off the result of variational minimization. In principle, DMC should give the exact energy irrespective of trial function. However, a poor choice of γ may give extremely slow convergence to the exact result.

III. RESULTS

A. Ground-state energy

The ground-state energy at several densities is listed in Table I. These results are in fair agreement with the DMC results of Ceperley and Alder,[17] though somewhat higher at small r_s. This small discrepancy is presumably due to differences in the size extrapolation. For high density this is an important correction, being as large as 0.008 74 Ry for the system of $N=200$ particles at $r_s=1$. There may also be differences in the convergence of the Ewald sums, discussed in the previous section. In the same Table we also compare our data with those reported by Hansen and Mazighi[3] and with those obtained through a self-consistent approach to dielectric screening (STLS).[14,16] Both of them are very close to the exact (DMC) result. The variational results of Hansen and Mazighi do not provide an upper bound on the energy in the thermodynamic limit because they have been computed with 128 particles without size extrapolation. In fact they are higher than our data at $N=128$ but at small r_s lie below our size-extrapolated values.

We have found that the following interpolation formula for $E_g(r_s)$ can reproduce both the correct asymptotic behaviors and the DMC data:

$$E_g(r_s)=-\{a_1r_s^{b_1}+a_2r_s^{b_2}+[a_3+a_3'\ln(r_s)]r_s^{b_3}+a_4r_s^{b_4}\}^c. \tag{3.1}$$

TABLE I. Ground-state energy E_g from DMC simulations compared with the results by Ceperley and Alder (Ref. 17) (CA), with the variational results by Hansen and Mazighi (Ref. 3) (HM) and with STLS results (Refs. 14 and 16) at different r_s. All values are in Rydberg; the digits in parentheses represent the error bar in the last decimal place. We also give the kinetic energy $\langle ke\rangle$ and the inverse compressibility $1/\rho K_T$ as obtained from Eq. (3.1).

r_s	E_g	CA	HM	STLS	$\langle ke\rangle$	$1/\rho K_T$
1	−0.776 64(5)	–	−0.7810	−0.771 240	0.175 264	−0.250 743
2	−0.451 92(3)	−0.4531(1)	−0.4547	−0.447 180	0.095 202	−0.148 866
5	−0.216 420(12)	−0.216 63(6)	−0.2170	−0.212 895	0.038 981	−0.074 351
10	−0.121 353(5)	−0.121 50(3)	−0.1216	−0.118 800	0.018 256	−0.043 501
20	−0.066 639(4)	−0.066 66(2)	−0.066 67	−0.064 864	0.007 999	−0.024 970
50	−0.029 276(3)	−0.029 27(1)	–	−0.028 220	0.002 509	−0.011 532
100	−0.015 4145(13)	−0.015 427(4)	−0.015 35	−0.014 733	0.000 998	−0.006 257
160	−0.009 9046(13)	–	–	–	0.000 517	−0.004 089

TABLE II. Parameters in Eq. (3.1) as determined by a least-squares fit with four free parameters and eight data points.

$a_1 = 7.085\,56$	$b_1 = 375/56$
$a_2 = 2.205\,75$	$b_2 = 417/56$
$a_3 = 0.251\,289$	$b_3 = 59/7$
$a_3' = -0.034\,817$	
$a_4 = 0.009\,236$	$b_4 = 125/14$
$c = -14/125$	

The parameters in Eq. (3.1) have been chosen so that for $r_s \to 0$ this formula reproduces the known limiting expression obtained by Brückner,[8]

$$E_g(r_s \to 0) \simeq -\frac{0.8031}{r_s^{3/4}} + 0.0280 + \cdots . \tag{3.2}$$

In the opposite limit $r_s \to \infty$ we only impose that the exponents of the two leading terms are -1 and $-3/2$, on the basis of the known asymptotic behavior for the crystal phase,[26,27]

$$E_g(r_s \to \infty) \simeq -\frac{1.791\,86}{r_s} + \frac{2.65}{r_s^{3/2}} . \tag{3.3}$$

Table II contains the final values of the parameters, which we regard as satisfactory since they correspond to a reduced χ^2 of 1.2. The fit is not significantly improved if we do not require c to be a "simple" rational number.

From the equation of state (3.1) one obtains an unbiased estimator (as opposed to the extrapolated estimator) for the kinetic energy via the virial theorem, $\langle ke \rangle = -d(r_s E_g)/dr_s$. The kinetic energy and the inverse compressibility $1/\rho K_T = -r_s^4 d[(E_g + \langle ke \rangle)/(9r_s^3)]/dr_s$ are also listed in Table I.

B. Dielectric response

Our results on the static dielectric function $\epsilon(k,0)$ are shown in Fig. 2. At low k our data are consistent with the compressibility sum rule,

$$\epsilon(k \to 0,0) \simeq \frac{4\pi e^2}{k^2} \rho^2 K_T . \tag{3.4}$$

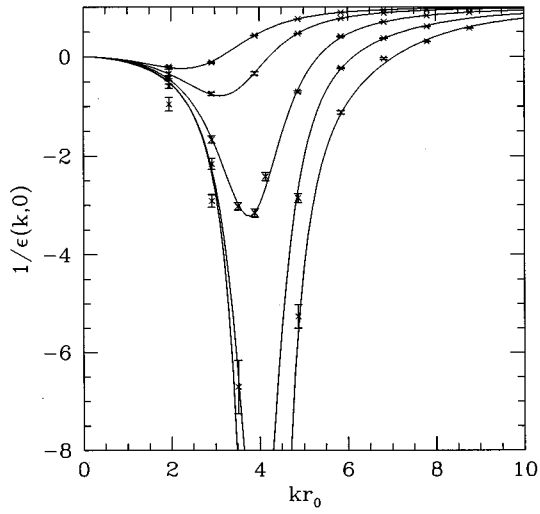

FIG. 2. Inverse static dielectric function $1/\epsilon(k,0)$ as a function of kr_0 for r_s = 10, 20, 50, 100, and 160. The solid lines are the fit given by Eqs. (3.5) and (3.10).

Given the well-established fact that the compressibility of the fluid of charged bosons is negative at all $r_s > 0$ (see also Table I), Eq. (3.4) ensures that $1/\epsilon(k,0)$ goes through a negative minimum before approaching unity as $k \to \infty$. This behavior implies overscreening of long-wavelength perturbations and does not lead to an instability of the boson plasma, owing to the presence of the rigid background. We remark from Fig. 2 that the minimum in $1/\epsilon(k,0)$ becomes deeper with decreasing density and its location approaches $kr_0 \simeq 4$, in approximate correspondence with the first star of reciprocal lattice vectors in the Wigner crystal.

From the DMC data on $\epsilon(k,0)$ we have obtained the static local-field factor $G(k)$ for exchange and correlation, using the relation[28]

$$\epsilon(k,0) = 1 - \frac{\frac{4\pi e^2}{k^2}\chi_0(k)}{1 + G(k)\frac{4\pi e^2}{k^2}\chi_0(k)} , \tag{3.5}$$

where $\chi_0(k)$ is the static susceptibility of the ideal boson gas,

TABLE III. DMC results for the static local-field factor $G(k)$ at different r_s. The digits in parentheses represent the error bar in the last decimal place.

kr_0	$r_s = 10$	$r_s = 20$	$r_s = 50$	$r_s = 100$	$r_s = 160$
1.9489	0.29(1)	0.36(3)	0.28(5)	0.38(2)	0.50(4)
2.9233	0.71(1)	0.73(1)	0.75(1)	0.74(1)	0.782(8)
3.5134	-	-	1.005(5)	0.997(9)	0.973(1)
3.8978	1.18(1)	1.21(2)	1.144(5)	1.107(3)	1.080(1)
4.1342	-	-	1.194(7)	1.148(3)	1.119(2)
4.8722	1.54(2)	1.47(1)	1.354(7)	1.210(6)	1.134(6)
5.8467	1.81(7)	1.54(2)	1.26(3)	1.161(7)	1.138(8)
6.8211	2.0(1)	1.53(3)	1.30(5)	1.22(2)	1.17(2)
7.7956	2.4(1)	1.84(8)	1.44(6)	1.53(4)	1.49(2)
8.7700	2.5(2)	2.1(1)	1.8(1)	-	1.75(5)

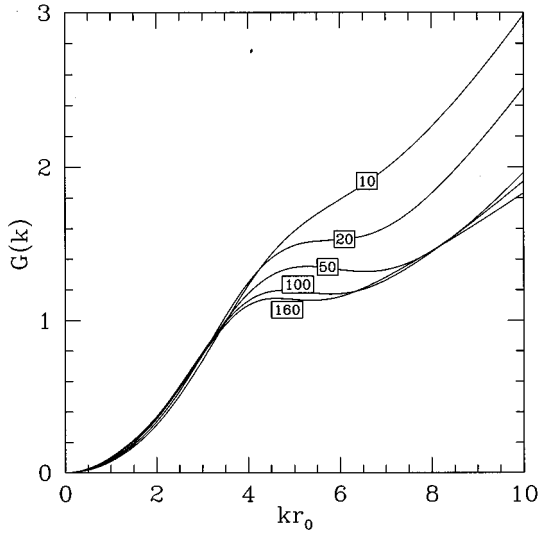

FIG. 3. Fitted form of the static local-field factor $G(k)$ at different r_s.

$$\chi_0(k) = -2\rho \frac{2m}{k^2}. \tag{3.6}$$

The function $G(k)$ is closely related to the exchange-correlation factor $f_{\rm xc}(k)$ entering density functional theory in the linear response approximation. In fact $4\pi e^2/k^2 G(k) = -f_{\rm xc}(k)$, where the Fourier transform of $f_{\rm xc}$ is defined through the exchange and correlation energy functional,

$$f_{\rm xc}(|\mathbf{r}-\mathbf{r}'|) = \left[\frac{\delta^2 E_{\rm xc}}{\delta\rho(\mathbf{r})\,\delta\rho(\mathbf{r}')}\right]_{\rho_0}. \tag{3.7}$$

The low-k behavior $G(k\to 0) \simeq -k^2/(4\pi e^2 \rho^2 K_T)$ is determined by the compressibility sum rule in Eq. (3.4), while the high-k limit is given by[29]

$$G(k\to\infty) \simeq \frac{4}{3}\frac{\langle ke\rangle}{\omega_{\rm pl}^2}\frac{k^2}{2m} + \frac{16}{5}\frac{\langle ke^2\rangle}{\omega_{\rm pl}^2} - \frac{16}{9}\frac{\langle ke\rangle^2}{\omega_{pl}^2} + \frac{2}{3}[1-g(0)]. \tag{3.8}$$

In Eq. (3.8), $\langle ke\rangle$ and $\langle ke^2\rangle$ are the average kinetic energy (see Sec. III A) and the average square kinetic energy, which is determined by the fourth moment of the momentum distribution. Our DMC results for $G(k)$ at various values of r_s are reported in Table III.

For charged fermions in the density range $2 \leqslant r_s \leqslant 10$ the DMC results on $G(k)$ (Ref. 30) show a very smooth cross-over from the low-k to the high-k behavior and can be interpolated with a one-parameter fit to the simple function

$$\frac{G(k)}{(kr_0)^2} = \left[(a-c)^{-n} + \left(\frac{(kr_0)^2}{b}\right)^n\right]^{-1/n} + c, \tag{3.9}$$

with a, b, and c given by the asymptotic expressions. Our data for charged bosons are consistent with this picture at $r_s = 10$, but at lower densities $G(k)$ develops a structure around $kr_0 \simeq 4$. Possibly neglecting fine details at very large k of presently unclear relevance, our DMC local-field factor is adequately described by simply adding a Gaussian term to the above expression, namely,

$$\frac{G(k)}{(kr_0)^2} = \left[(a-c)^{-n} + \left(\frac{(kr_0)^2}{b}\right)^n\right]^{-1/n} + c + d\exp\left(-\frac{(k-k_0)^2 r_0^2}{2\sigma^2}\right). \tag{3.10}$$

Fitting this four-parameter expression to the DMC data results in the curves shown in Figs. 2 and 3, with the values of the parameters given in Table IV.

We remark that at $kr_0 \simeq 4$ the structure seen in Fig. 3 for $G(k)$ in the low density regime is not peculiar to the boson fluid. Unpublished data for the polarized electron gas at crystallization density exhibit a similar behavior in both two and three dimensions.[31]

Finally, in Fig. 4 we compare our data for $G(k)/k^2$ at $r_s = 10$ with its asymptotic behaviors and with the values obtained from the results of Sugiyama, Bowen, and Alder.[18] Their result at $k \simeq 2$ is compatible with ours within statistical errors. The situation at $r_s = 100$ is completely similar. Figure 4 also shows the results of approximate theories, obtained from the Jastrow approach[12] and from the self-consistent VS approach to dielectric screening.[16] The VS curve from Ref. 16 incorporates the correct long-wavelength behavior, but is not quantitatively correct at higher wave number. The variational calculation by Saarela,[12] which incorporates both asymptotic behaviors, is in remarkably good agreement with our DMC data at all wave numbers considered.

C. Momentum distribution

As mentioned in Sec. II we have obtained DMC data for $n(k)$ corresponding to values of $\mathbf{k}$ on the reciprocal lattice of the simulation box and for its Fourier transform $n(r)$. Some of these results are shown in Figs. 5 and 6. We have collected this information in a fitting formula incorporating the known asymptotic behaviors.

At high k the tail of the momentum distribution $n(k)$ is given by the cusp condition[32]

TABLE IV. Values of the fit parameter for the static local-field factor $G(k)$, after Eq. (3.10).

r_s	a	b	c	d	n	$k_0 r_0$	σ
10	0.071 85	0.958 64	0.020 274	0.012 929	3.057	3.666 36	1.498 06
20	0.080 61	0.955 23	0.017 769	0.037 192	0.7825	3.463 74	1.504 38
50	0.084 26	0.977 56	0.013 933	0.048 478	0.5435	2.988 19	1.779 83
100	0.101 35	1.029 61	0.011 078	0.037 348	0.7333	3.096 35	1.372 73
160	0.108 78	1.016 62	0.009 191	0.026 138	0.9670	3.317 96	1.093 57

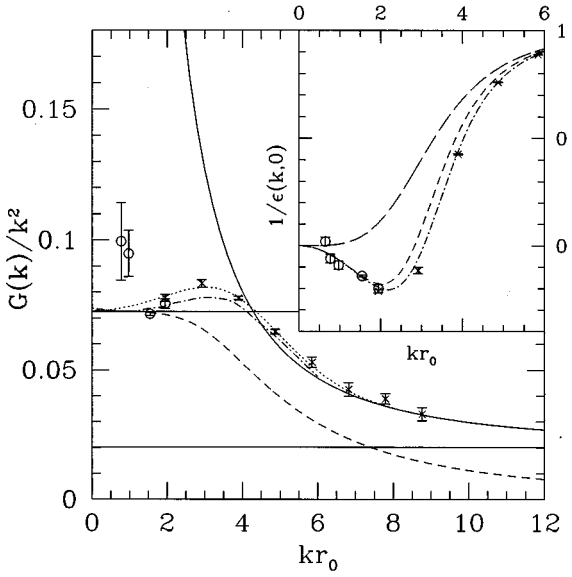

FIG. 4. Static local-field factor $G(k)$ over k^2 at $r_s=10$ (crosses with error bars), compared with the asymptotic expressions (full lines), with the fit (dotted line) and with previous results by other authors. The circles with error bars are the values obtained from the data of Sugiyama, Bowen, and Alder (Ref. 18), the dashed line gives the VS (Vashishta-Singwi) results from Ref. 16, and the dot-dashed line the variational calculation by Saarela (Ref. 12). The corresponding inverse static dielectric function $1/\epsilon(k,0)$ is plotted in the inset, omitting the asymptotic behaviors and the fit and including the RPA curve (long-dashed line).

$$n(k\to\infty)\simeq\frac{9r_s^2g(0)}{(kr_0)^8}. \tag{3.11}$$

In the opposite low-k limit $n(k)$ diverges with a behavior given by quantum hydrodynamics:[33]

$$n(k\to0)\simeq n_0\frac{2m\omega_{\rm pl}}{4k^2}+\frac{m^2n_0\omega_{\rm pl}^2}{64\rho k}+O(1), \tag{3.12}$$

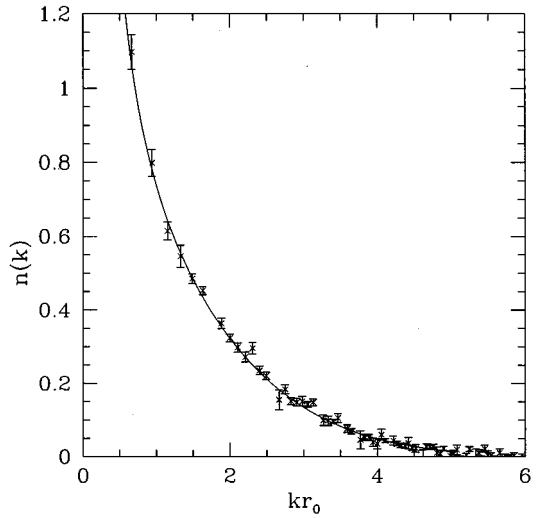

FIG. 5. DMC results for the momentum distribution $n(k)$ at $r_s=100$, compared with the fit given by Eq. (3.13).

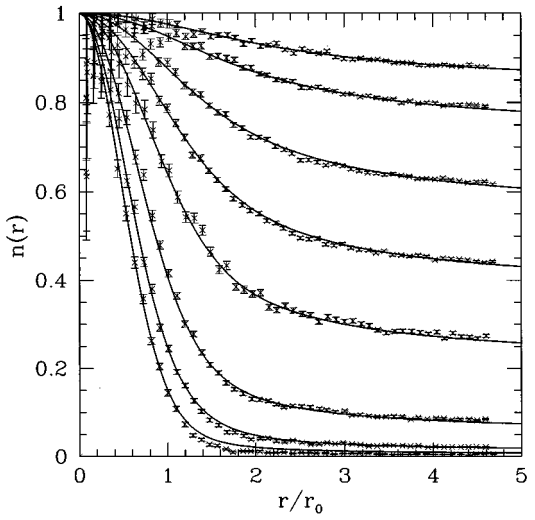

FIG. 6. DMC data and fitted expression for the one-body density matrix at r_s = 1, 2, 5, 10, 20, 50, 100, and 160 (from top to bottom).

where n_0 is the condensate fraction. Harmonic theory for the crystalline phase predicts a Gaussian momentum distribution, determined by the zero-point phonon energy. We expect that this behavior should be reflected in that of the liquid close to the transition.

We have therefore chosen the following expression to interpolate the DMC data:

$$n(k)=(2\pi)^3n_0\rho\delta^3(k)+\frac{a_0}{k^2(k^2+a_1^2)^3}+\left(\frac{a_4}{k^2}+\frac{a_5}{k}+a_6\right)\exp\left\{-\frac{(k-a_3)^2-a_3^2}{2a_2^2}\right\}. \tag{3.13}$$

Given the known values of the density and the mean kinetic energy, as well as the known asymptotic behaviors, the remaining parameters are determined by a least-squares fit to the DMC data. We set the parameter a_3 equal to zero when this choice is compatible with the data (as seen from χ^2 values), so that the number of fitted parameters is three or four depending on r_s. The fit was performed on both the k-space points and their Fourier transform, the one-body density matrix. In the fitting procedure we have included only the values of $n(r)$ obtained from random displacements of particles, as mentioned in Sec. II. In fact, the value obtained by fixed increments is more accurate for small r; however, in this region it basically gives the extrapolated estimator of the kinetic energy, and we prefer to enforce instead the unbiased estimator of $\langle ke\rangle$ of Sec. III A. In order to give the same weight to real space and to reciprocal space the function we minimized was the sum of the two reduced χ^2 values, which were in the range from 0.3 to 2.5 for all r_s except at $r_s=160$. Table V contains the best-fit parameters and the resulting values of n_0 and $\langle ke^2\rangle$.

Figure 5 shows the k-space data and the fitted curve for $r_s=100$, while Fig. 6 shows the resulting $n(r)$ at various values of r_s. The $r\to\infty$ limiting value of $n(r)$ gives the condensate fraction.

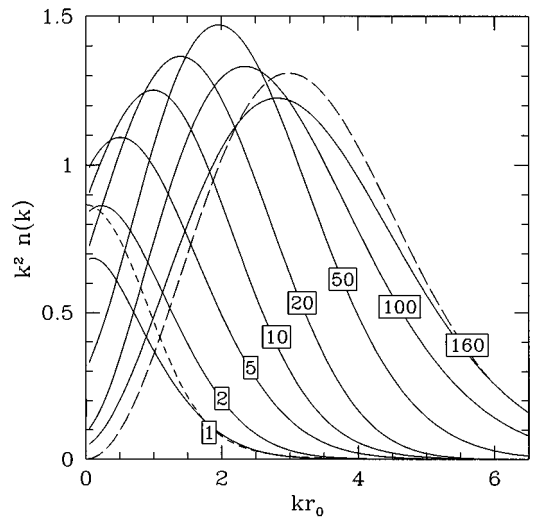

FIG. 7. Momentum distribution at various values of r_s compared with Foldy's results at $r_s=1$ (short-dashed curve) and with a Maxwell distribution at $r_s=160$ (dashed curve). We plot $k^2n(k)$ for greater clarity.

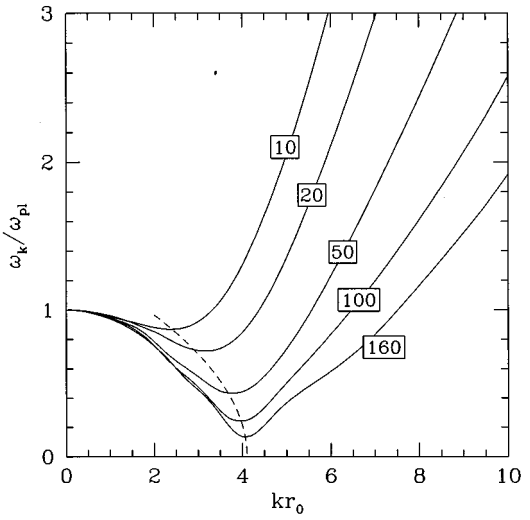

FIG. 9. Upper bound on the plasmon dispersion curve as derived from the static susceptibility and the static structure factor, for r_s = 10, 20, 50, 100, and 160. The dashed line shows the position of the minimum in the various curves.

Figure 7 shows the resulting expressions for $k^2n(k)$ at various values of r_s. At $r_s=1$ the Bogoliubov curve[7] is almost correct, as could be expected from the fact that the condensate fraction is above 80%. This is consistent with the usual picture of $r_s\to 0$ as the "uniform" (or RPA) limit. With growing r_s the shape of the curves changes qualitatively, with exchange effects playing a minor role at low density. At the crystallization density ($r_s=160$) less than 1% of the particles are in states with occupation number larger than one and the resulting momentum distribution is similar to the Maxwell-Boltzmann distribution taken at a fictituous temperature given by $\langle ke\rangle = 3/2\, k_BT$.

D. Structure factor

The static structure factor $S(k)$ has been obtained by Fourier transforming the DMC data on the pair distribution function $g(r)$ as given by the simulation for $r<L/2$, with L the side of the simulation box, after extending the data for $r>L/2$ with an oscillatory, decreasing tail of the form $ar^{-b}\sin[c(r-r_0)]$. The parameters a, b, c, and r_0 are fitted to the higher-r part of the data. This procedure gives reliable results for intermediate and high k, but does not reproduce very well the limit $k\to 0$ since it does not contain any normalization condition. The resulting $S(k)$ is then smoothly matched to the correct asymptotic behavior for $k\to 0$, the result being shown in Fig. 8. A strong peak at $kr_0\simeq 4$ develops as the crystallization density is approached.

The statistical errors in $S(k)$ are estimated to be less than 1%, smaller than the systematic errors coming from the use of extrapolated estimators (see Sec. II) and from the tail added to $g(r)$. The final precision can be estimated to be of a few percent.

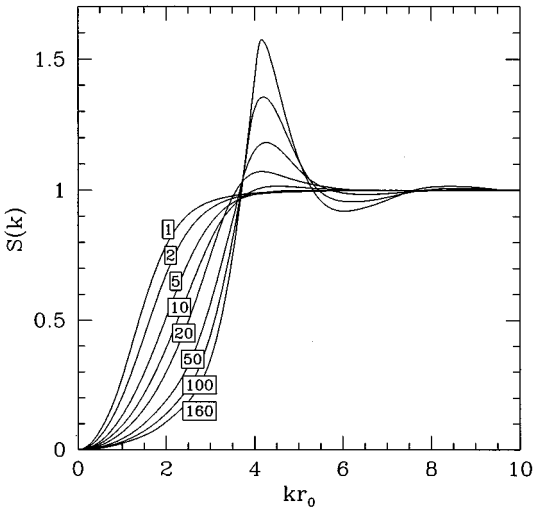

FIG. 8. Static structure factor $S(k)$ as a function of kr_0 for r_s = 1, 2, 5, 10, 20, 50, 100, and 160.

E. An upper bound on the plasmon dispersion curve

The so-called sum-rules approach has given useful information on excitations in liquid ^{4}He.[34] A first application of this method to the boson plasma has led to the rigorous conclusion that the leading dispersion coefficient of the plasmon excitation is negative for all values of $r_s>0$.[35] In this section we display a rigorous upper bound on the whole plasmon dispersion curve, from our simulation results on $\chi(k)$ and $S(k)$.

We define the moments of the frequency-dependent density response function as

$$m_n(k)=-\frac{2}{\pi}\int_0^\infty \mathrm{Im}\chi(k,\omega)\omega^n d\omega. \tag{3.14}$$

If $\omega_k^{\min}$ is the energy of the lowest eigenstate excited by the operator $\rho_k=\Sigma_q a_q^\dagger a_{q+k}$, the following relation holds:[36]

$$\omega_k^{\min}\leqslant \frac{m_0(k)}{m_{-1}(k)}=-\frac{2\rho S(k)}{\chi(k)}. \tag{3.15}$$

TABLE V. Fitted values for the parameters in Eq. (3.13).

r_s	1	2	5	10	20	50	100	160
n_0	0.827	0.722	0.542	0.359	0.206	0.053	0.0104	0.004
$\langle ke^2 \rangle$	0.745	0.115	0.00863	0.00122	0.000167	1.24×10^{-5}	2.05×10^{-6}	4.72×10^{-7}
a_0	3.8	8.64	12.4	-	-	-	-	-
a_1	1.45	1.75	2.6	-	-	-	-	-
a_2	1.03	1.12	1.3	1.1	1.07	1.5	2.59	2.35
a_3	-	-	0.105	1.3	1.57	0.754	-3.03	-0.77
a_4	0.264	0.531	0.902	0.938	0.693	0.325	0.0901	0.0438
a_5	0.153	0.267	0.422	-0.334	-0.247	0.412	0.245	0.132
a_6	-0.028	-0.0481	-0.0817	0.0615	0.0639	0.165	0.919	0.417

The value of the upper bound in Eq. (3.15) has been obtained by using the fluctuation-dissipation theorem and the Kramers-Kronig relations. This upper bound becomes an equality when the spectrum consists of a single pole, i.e., for $k\rightarrow 0$.

Figure 9 displays the upper bound of Eq. (3.15) at various values of r_s. In the case of liquid ^{4}He direct comparison with experimental data[34] shows that, while the Feynman result is about a factor of 2 higher than the roton minimum, the bound given by Eq. (3.15) is only 30% too high. However, as for ^{4}He one may expect that the approach of the upper bound to the single particle recoil frequency at high k is qualitatively incorrect.

We also notice from Fig. 9 that with increasing r_s the minimum in the upper bound decreases down to very low frequency in approximate correspondence with the first Brillouin zone edge of the Wigner crystal.

IV. SUMMARY AND CONCLUDING REMARKS

We have presented a systematic study of the properties of the charged boson fluid at $T=0$ by diffusion Monte Carlo. We have given a simple analytical expression for the internal energy of the fluid as a function of coupling strength r_s, from which reliable results for the equation of state can be obtained in the whole fluid density range $0\leqslant r_s\leqslant 160$. Our results for the static density response function cover the relevant region of wave numbers and show significant changes in the response as the fluid approaches crystallization density. An analytical interpolation of these data has also been given. Similar features emerge from the data on the structure factor. The shape of the momentum distribution changes significantly in the evolution of the system from the uniform limit ($r_s<1$) to the strongly coupled fluid regime ($r_s\simeq 160$), paralleling the decrease of the condensate fraction from 83% to less than 1%. These data have also been summarized in an interpolation formula consistent with the known asymptotic behaviors. As an application we have presented a rigorous upper bound on the plasmon dispersion curve, which shows the presence of a deep minimum in the strong coupling regime.

ACKNOWLEDGMENTS

The simulations presented in this work have been carried out on the computing facilities of CNUCE, which is supported by the Consiglio Nazionale delle Ricerche and by the Ministero dell'Università e della Ricerca Scientifica e Tecnologica of Italy. This work was performed as part of the activities of FORUM-INFM Institute for Condensed Matter Theory.

[1] F. Y. Wu and E. Feenberg, Phys. Rev. **128**, 943 (1962).
[2] R. Monnier, Phys. Rev. A **5**, 814 (1972).
[3] J. P. Hansen and R. Mazighi, Phys. Rev. A **18**, 1282 (1978).
[4] M. R. Schafroth, Phys. Rev. **96**, 1149 (1954).
[5] A. S. Alexandrov and N. F. Mott, Supercond. Sci. Technol. **6**, 215 (1993).
[6] B. W. Ninham, Phys. Lett. **4**, 278 (1963).
[7] L. L. Foldy, Phys. Rev. **124**, 649 (1961).
[8] K. A. Brückner, Phys. Rev. **156**, 204 (1967).
[9] S. K. Ma and C. W. Woo, Phys. Rev. **159**, 165 (1967).
[10] D. K. Lee, Phys. Rev. **187**, 326 (1969).
[11] D. K. Lee and F. H. Ree, Phys. Rev. A **5**, 814 (1972).
[12] M. Saarela, Phys. Rev. B **29**, 191 (1984).
[13] S. R. Hore and N. E. Frankel, Phys. Rev. B **12**, 2619 (1975).
[14] A. Caparica and O. Hipólito, Phys. Rev. A **26**, 2832 (1982).
[15] A. Gold, Z. Phys. B **89**, 1 (1992).
[16] S. Conti, M. L. Chiofalo, and M. P. Tosi, J. Phys. Condens. Matter **6**, 8795 (1994).
[17] D. M. Ceperley and B. J. Alder, Phys. Rev. Lett. **45**, 566 (1980).
[18] G. Sugiyama, C. Bowen, and B. J. Alder, Phys. Rev. B **46**, 13 042 (1992).
[19] D. M. Ceperley and B. J. Alder, J. Phys. (Paris) Colloq. **7**, C295 (1980).
[20] P. J. Reynolds, D. M. Ceperley, B. J. Alder, and W. A. Lester, J. Chem. Phys. **77**, 5593 (1982).
[21] C. J. Umrigar, M. P. Nightingale, and K. J. Runge, J. Chem. Phys. **99**, 2865 (1993).
[22] D. M. Ceperley, Phys. Rev. B **18**, 3126 (1978).
[23] V. Natoli and D. Ceperley, J. Comput. Phys. **117**, 171 (1995).
[24] D. M. Ceperley and M. H. Kalos, in *Monte Carlo Methods in Statistical Physics*, edited by K. Binder (Springer, Berlin, 1979).
[25] S. Moroni, D. M. Ceperley, and G. Senatore, Phys. Rev. Lett. **69**, 1837 (1992).
[26] H. R. Glyde, G. H. Keech, R. Mazighi, and J. P. Hansen, Phys. Lett. **58A**, 226 (1978).
[27] W. J. Carr, Jr., Phys. Rev. **122**, 1437 (1961).

[28] K. S. Singwi and M. P. Tosi, Solid State Phys. **36**, 177 (1981).
[29] A. Holas, in *Strongly Coupled Plasma Physics*, edited by F. J. Rogers and H. E. DeWitt (Plenum Press, New York, 1986), p. 463.
[30] S. Moroni, D. Ceperley, and G. Senatore, Phys. Rev. Lett. **75**, 689 (1995).
[31] S. Moroni (unpublished).
[32] J. C. Kimball, J. Phys. A **8**, 1513 (1975).
[33] S. Giorgini and S. Stringari (unpublished).
[34] J. Boronat, J. Casulleras, F. Dalfovo, S. Moroni, and S. Stringari, Phys. Rev. B **52**, 1236 (1995).
[35] M. L. Chiofalo, S. Conti, S. Stringari, and M. P. Tosi, J. Phys. Condens. Matter **7**, L85 (1995).
[36] F. Dalfovo and S. Stringari, Phys. Rev. B **46**, 13 991 (1992).